

AD-A161 666

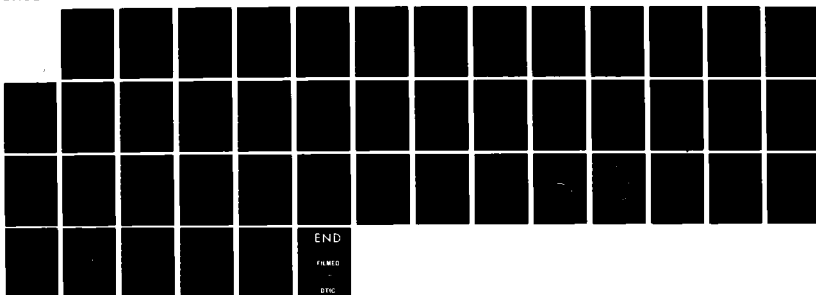
TWO-DIMENSIONAL STRAIN CYCLING IN PLASTICITY(U)
CALIFORNIA UNIV BERKELEY DEPT OF MECHANICAL ENGINEERING
P H NAGHDI ET AL. NOV 85 UCB/AM-85-1 N00014-84-K-0264

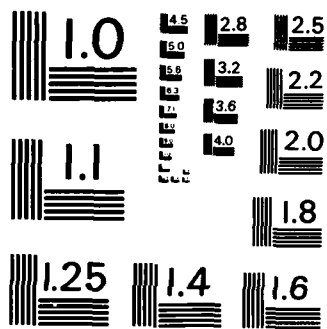
1/1

UNCLASSIFIED

F/G 11/6

NL





MICROCOPY RESOLUTION TEST CHART
NATIONAL BUREAU OF STANDARDS-1963-A

AD-A161 666

JTG FILE COPY

SECURITY CLASSIFICATION OF THIS PAGE (When Data Entered)

REPORT DOCUMENTATION PAGE		READ INSTRUCTIONS BEFORE COMPLETING FORM
1. REPORT NUMBER UCB/AM - 85 - 1	2. GOVT ACCESSION NO.	3. RECIPIENT'S CATALOG NUMBER
4. TITLE (and Subtitle) Two-Dimensional Strain Cycling in Plasticity		5. TYPE OF REPORT & PERIOD COVERED
AUTHOR(s) P. M. Naghdi and D. J. Nikkel Jr.		6. PERFORMING ORG. REPORT NUMBER
PERFORMING ORGANIZATION NAME AND ADDRESS Department of Mechanical Engineering University of California Berkeley, CA 94720		8. CONTRACT OR GRANT NUMBER(s) N00014-84-K-0264
1. CONTROLLING OFFICE NAME AND ADDRESS Mechanics Division, Solid Mechanics Program Office of Naval Research 800 N. Quincy St., Arlington, VA 22217		10. PROGRAM ELEMENT, PROJECT, TASK AREA & WORK UNIT NUMBERS 064-436
14. MONITORING AGENCY NAME & ADDRESS (if different from Controlling Office)		12. REPORT DATE 11/85
		13. NUMBER OF PAGES
		15. SECURITY CLASS. (of this report)
		15a. DECLASSIFICATION/DOWNGRADING SCHEDULE
16. DISTRIBUTION STATEMENT (of this Report) Approved for public release; distribution unlimited		
17. DISTRIBUTION STATEMENT (of the abstract entered in Block 20, if different from Report) NOV 29 1985		
18. SUPPLEMENTARY NOTES		
19. KEY WORDS (Continue on reverse side if necessary and identify by block number) Strain cycling, two-dimensional, strain-space formulation of plasticity, theoretical predictions, comparison with experiments, saturation hardening, erasure memory.		
20. ABSTRACT (Continue on reverse side if necessary and identify by block number) Detailed calculations are presented for strain cycling in a homogeneous deformation that can be sustained by a biaxial state of stress in thin-walled specimens of OFHC copper. These calculations are made with a set of relatively simple constitutive equations within the framework of the strain-space formulation of plasticity. The predicted theoretical calculations, carried out in the context of small deformation, are in good agreement with corresponding available experimental results for saturation hardening and erasure of memory in two-dimensional strain cycling. Also, with the use of the calculated results, a		

DD FORM 1473

1 JAN 73

EDITION OF 1 NOV 65 IS OBSOLETE

S/N 0102-LF-014-6601

SECURITY CLASSIFICATION OF THIS PAGE (When Data Entered)

85 11 25 057

scalar quantity that characterizes strain-hardening is plotted as a function of plastic strains. Such plots are likely to be useful for computational purposes.

Two-dimensional Strain Cycling in Plasticity

by

P. M. Naghdi and D. J. Nikkel, Jr.

Department of Mechanical Engineering
University of California, Berkeley, CA 94720

Abstract Detailed calculations are presented for strain cycling in a homogeneous deformation that can be sustained by a biaxial state of stress in thin-walled specimens of OFHC copper. These calculations are made with a set of relatively simple constitutive equations within the framework of the strain-space formulation of plasticity. The predicted theoretical calculations, carried out in the context of small deformation, are in good agreement with corresponding available experimental results for saturation hardening and erasure of memory in two-dimensional strain cycling. Also, with the use of the calculated results, a scalar quantity that characterizes strain-hardening is plotted as a function of plastic strains. Such plots are likely to be useful for computational purposes.

↑



1. Introduction

In an interesting series of experiments pertaining to two-dimensional strain cycling in plasticity that can be sustained by a biaxial state of stress resulting from combined tension-compression and torsion in thin-walled specimens of OFHC copper[†], Lamba and Sidebottom (1978a,b) observed the following three phenomena:

- a) The occurrence of saturation hardening after loading from an undeformed state and cycling along a strain path which is essentially an ellipse in the normal strain-shear strain plane;
- b) the erasure of memory after the material has reached a state of saturation; and
- c) the nature of the post-saturation stress response for cycling in a relatively "complex" nonproportional strain path.

With reference to the above two-dimensional strain cycling experiments, our main objective is to examine the predictive capability of a (rate-independent) theory of plasticity formulated in a strain space setting with the use of special constitutive equations employed previously by Naghdi and Nikkel (1984). Also, by employing the strain-hardening characterization which arises in the strain-space formulation of plasticity (Casey and Naghdi, 1981, 1983, 1984a) and which is represented by a scalar function ϕ , we calculate (over the domain of interest) the values of ϕ for the material used in the experiments of Lamba and Sidebottom (1978a,b) and plot this as a function of plastic strains. As in the experiments of Lamba and Sidebottom (1978a,b), our calculations are carried out in the context of small deformation.

[†]The abbreviation OFHC stands for "oxygen-free high conductivity."

In a previous paper (Naghdi and Nikkel, 1984) comparisons were made between the predictions of uniaxial stress and strain cycling in plasticity and corresponding available experiments. The previous calculations (Naghdi and Nikkel, 1984) were carried out in a strain space setting by means of special constitutive equations obtained on the basis of a theory first formulated relative to stress space by Green and Naghdi (1965, 1966) and subsequently reformulated relative to strain space by Naghdi and Trapp (1975a), along with some additional developments pertaining to loading criteria and hardening characterization by Casey and Naghdi (1984a,b).

Description of the Strain Cycling Problem

As in the experiments of Lamba and Sidebottom (1978a,b), we consider the combined tension-compression and torsion of a thin-walled circular cylinder whose axis is in the x_1 -direction. As usual, we neglect the variation of stress and strain in the radial coordinate direction so that the stress and strain components referred to cylindrical polar coordinates are then independent of position. We denote the axial stress and axial strain, respectively, by s_{11} and e_{11} ; and similarly denote the shear stress and shear strain, respectively, by s_{12} and e_{12} .

The analysis in Section 3 and the procedure for calculations in Section 4 require a reduction of the general loading criteria since not all components of strain (and strain rate) are known a priori in the context of the particular experiment considered. This reduction is discussed in Appendix A and the results are employed in all calculations of Section 4. Our calculations do not include those appropriate for two-dimensional stress

cycling, even though it is relatively easier to calculate such cycles for materials exhibiting hardening behavior.*

In the remainder of this section, we discuss in some detail the main features of the calculated results. A summary of the calculations can be arranged in three groups corresponding to the nonproportional strain cycling experiments of Lamba and Sidebottom (1978a,b) as listed in the opening paragraph of this section. The first experiment pertains to saturation hardening after loading from an undeformed state, and the second two concern the behavior after the material has reached a state of saturation. In each case, the strain path in the e_{11} - e_{12} plane is the input to the problem, and the stress response (s_{11} and s_{12}) is calculated from the relevant constitutive equations. A graphical presentation of the calculated stress trajectory in the s_{11} - s_{12} plane alone does not give all the relevant information, unless a knowledge of the correspondence between all points of the stress trajectory and all points of the input strain path in the e_{11} - e_{12} plane is also known. It is therefore, necessary to also plot the calculated results in either the s_{11} - e_{11} or the s_{12} - e_{12} plane. For clarity's sake, we have presented the calculated results in both the s_{11} - e_{11} and s_{12} - e_{12} planes.

Saturation Hardening

For two-dimensional saturation hardening, we prescribe e_{11} and e_{12} parametrically as functions of time such that in the e_{11} - e_{12} plane the strain path is as depicted in the inset of Fig. 1(a). This

*This is because for materials exhibiting hardening behavior the loading criteria in stress space may be used (Casey and Naghdi, 1984b), and for two-dimensional stress cycling all of the components of stress are prescribed in contrast to two-dimensional strain cycling where some of the components of strain are not known a priori.

corresponds to uniaxial tensile loading from the undeformed state until the axial strain reaches the value 0.00635 (point Q in Fig. 1(a)) followed by combined tension-compression and torsion controlled in such a way that e_{11} and e_{12} cycle in a counterclockwise direction around the nearly elliptical path in the inset of Fig. 1(a).⁵ The strain components e_{11} and e_{12} were parametrically specified to be sinusoidal differing by a 90 degree phase shift. The calculated results for stresses are shown in Figs. 1(a-c) along with the experimental curves for the first few cycles only, since the portion of the trajectory for additional cycles would crowd the figure. Figure 1(a) represents the stress trajectory and Figs. 1(b,c) are alternative representations of the calculations in the s_{11} - e_{11} and s_{12} - e_{12} planes. Points corresponding to Q,R,S,T on the prescribed strain path in the inset of Fig. 1(a) have been labeled in Figs. 1(a-c) only for the portion of the path which represents a cycle at saturation and not for prior cycles. These results are in good qualitative agreement with the experimental results of Lamba and Sidebottom (1978a). In agreement with the experimental results, the theory predicts that saturation occurs after about four cycles. The main differences between the theoretical predictions and the experimental results are that the predicted maximum shear stress at saturation (point R in Figs. 1(a,c)) is slightly greater than the corresponding experimental value while the predicted maximum axial stress at saturation (point T in Figs. 1(a,b)) is slightly less than the corresponding experimental value. The reasons for these differences are discussed in Section 5.

⁵The actual experimental strain path in Fig. 3(a) of Lamba and Sidebottom (1978a) is not perfectly elliptical. In the present calculations the portion of the path in the upper half of the e_{11} - e_{12} plane is specified to be the upper half of an ellipse with vertices on the e_{11} axis at -0.00623 and 0.00635 and a semiaxis of 0.00531 in the e_{12} direction. The portion of the path in the lower half of the e_{11} - e_{12} plane is specified to be the lower half of an ellipse with the same vertices on the e_{11} axis, but with a semiaxis of 0.00588 in the e_{12} direction.

Erasure of Memory

Consider next the erasure of memory property observed by Lamba and Sidebottom (1978a) in the case of OFHC copper. The phenomenon occurs when the material has reached a state of saturation after strain cycling along an elliptical path in the e_{11} - e_{12} plane. If subsequent linear strain paths lie within the elliptical strain path (which was originally used to reach the state of saturation), then corresponding to a given linear path in the e_{11} - e_{12} plane there is a particular limiting stress cycle response in the s_{11} - s_{12} plane. This process is repeated as the material is cycled again along the strain path. Lamba and Sidebottom (1978a) observed that a larger cycle (not necessarily along a linear path) in the e_{11} - e_{12} plane essentially erases the effect of any previously traversed smaller cycles and returns the material to a state in which the limiting stress cycle response corresponds to that of the larger cycle. With the use of the linear strain paths BDB and BFB (as the larger and smaller cycles) indicated in the inset of Fig. 2(a), a calculation leading to a state of saturation was arrived at by first cycling in shear along $B'D'B'$ for four cycles followed by cycling along $B'CD'EB'$ for an additional four cycles. Then, the effect of erasure of memory was calculated by further cycling which alternates along BDB and BFB. The results of calculations are shown in Figs. 2(a-c) along with the experimental curves from Lamba and Sidebottom (1978a, Figs. 5(b,c)), where for clarity only the portion of the response corresponding to cycling which alternates along BDB and BFB are indicated.^{§§} The erasure of memory phenomenon is best seen in Fig. 2(c), where

^{§§} In Lamba and Sidebottom (1978a), at the point we've labeled D, the value of the shear strain shown in Fig. (5a) (the strain path in the axial strain - shear strain plane) is somewhat different from its value shown in Fig. (5b) (the experimental results shown in the shear stress-shear strain plane). In prescribing the strain path for our calculations, in order to compare with the experimental results we specified the value of the shear strain at point D to be that indicated in Fig. (5b) of Lamba and Sidebottom (1978a).

along the segment of path BD the effect of the path BFB has become undetectable by the time the trajectory has reached point D. Thus, the larger cycle BDB erases the material's memory of the previously traversed smaller cycle BFB. In addition, the overall response is in qualitative agreement with the experimental results of Lamba and Sidebottom (1978a), while the predicted shear stress is again higher than the corresponding experimental results (Fig. 2(c)) and the predicted compressive axial stress has a larger absolute value than the corresponding experimental results (Fig. 2(b)). Also, the slope of the calculated s_{12} - e_{12} curve in Fig. 2(c) during loading along FB is different than on the corresponding experimental curve. Again, these differences are discussed in some detail in Section 5.

Complex Nonproportional Strain-Path

Now, with reference to the third experiment of Lamba and Sidebottom (1978b), consider the predicted response for a "complex" nonproportional strain path (using the terminology of Lamba and Sidebottom) applied after the material has reached a state of saturation. The state of saturation is attained in the same way as discussed earlier in the preceding paragraph, namely by cycling first in shear followed by cycling along an elliptical path in the e_{11} - e_{12} plane. After this, a path was prescribed which returned e_{11} and e_{12} to the origin of the e_{11} - e_{12} plane (point O in Fig. 3(a)) while at the same time the plastic strains were returned to the value zero.* Next let e_{11} and e_{12} be

*This calculation was performed by prescribing a path unloading from the elliptical path at a point such as B' in the insert of Fig. 2(a) on which $e_{11}=0$ and allowing reverse loading to take place until such a point where $e_{12}^p=0$. At this point e_{11} has also become essentially zero which is again indicative of erasure of memory. Reversing the direction along this path until point O in Fig. 3(a) is reached results in only elastic behavior.

prescribed parametrically as functions of time such that in the e_{11} - e_{12} plane the strain path is represented by the linear segments 0-1, 1-2, 2-3, . . . , 7-8 in the inset of Fig. 3(a). The calculated results for stresses are shown in Figs. 3(a-c) which qualitatively agree well with the experimental results of Lamba and Sidebottom (1978b, Figs. 2(a-d)). Moreover, the theory again predicts the erasure of memory effect since as the path 0-1, . . . , 7-8 in the inset of Fig. 3(a) is traversed a second time, the stress path becomes indistinguishable from the first time the path was traversed. Thus, the larger path 6-7-8 erases the effect of the previously traversed smaller portion of the path 1-6.

Strain Hardening Behavior - The Function ϕ

In view of the fundamental role played by a scalar function ϕ that characterizes strain-hardening behavior of the material (Casey and Naghdi, 1984a), we represent ϕ as a surface which exhibits the nature of strain-hardening at any elastic-plastic state with fixed values of the total strain components[†] e_{11} and e_{12} . The surface in Fig. 4 is a plot of ϕ (defined in Eq. (2.10)) as a function of the plastic strains e_{11}^p and e_{12}^p for fixed values of the total strains e_{11} and e_{12} prescribed in the course of calculations; in the plot of Fig. 4 the prescribed total strains are specified to be $e_{11}=e_{12}=0$. For different values of e_{11} and e_{12} , the surface represented by ϕ merely translates parallel to the plane of e_{11}^p - e_{12}^p . A choice of the total strains, say $(\bar{e}_{11}, \bar{e}_{12})$, specifies a particular surface and elastic-plastic states reached by different strain paths ending at $(\bar{e}_{11}, \bar{e}_{12})$ will in general correspond to different points on the surface ϕ . The outer boundary of this surface (which has the smallest value of ϕ) corresponds to the state of saturation, while the inner boundary corresponds to the largest value that ϕ can take in the domain

[†]A topographical representation of this kind was used recently in a different context by Casey and Lin (1983).

of interest. A further discussion of how the surface was calculated is found at the end of Section 4. As is evident from the plot in Fig. 4, ϕ is always positive; and hence, in view of the conditions for strain-hardening characterization (see for example the conditions (8) in Naghdi and Nikkel, 1984), the material always exhibits hardening behavior.[†] It also shows how ϕ decreases with additional plastic deformation, taking its largest value at initial yield and its smallest value at saturation. The value of ϕ is constant at both initial yield and saturation.

[†]It should be emphasized that even though one component of the stress may be decreasing during loading while the corresponding strain component is increasing (e.g., as in Fig. 2(b)) the material is not exhibiting softening behavior in two-dimensional cycling.

2. General Background and Special Constitutive Equations

With reference to a strain-space formulation of plasticity and for the special constitutive equations used previously (Naghdi and Nikkel 1984), we include here a brief summary of the relevant equations of the purely mechanical theory contained in the papers of Green and Naghdi (1965, 1966), Naghdi and Trapp (1975a) and Casey and Naghdi (1981, 1983)[†].

In the context of infinitesimal deformation, we recall that the main ingredients of the rate-type theory of plasticity, in addition to the total strain e_{KL} , are plastic strain e_{KL}^p and a measure of work-hardening κ . Also, no distinction needs to be made between various measures of stress which we denote by s_{KL} . As usual, it is convenient to express the various constitutive response functions in terms of the components of deviatoric stress τ_{KL} and deviatoric strain γ_{KL} , namely

$$\begin{aligned}\tau_{KL} &= s_{KL} - \bar{s} \delta_{KL} \quad , \quad \tau_{KK} = 0 \quad , \\ \gamma_{KL} &= e_{KL} - \bar{e} \delta_{KL} \quad , \quad \gamma_{KK} = 0 \quad ,\end{aligned}\tag{2.1}$$

with a similar definition for the deviatoric plastic strain γ_{KL}^p , where \bar{s} , \bar{e} and \bar{e}^p denote the mean normal stress, mean normal strain, and mean normal plastic strain, respectively. For materials which are isotropic in reference configuration and in the presence of plastic incompressibility ($\bar{e}^p = 0$), we specify the stress response by generalized Hooke's law and the loading functions g and f in strain space and stress space, respectively, by[§]

[†] A more expanded summary is contained in Sections 2 and 3 of Naghdi and Nikkel (1984).

[§] The loading functions in (2.2) with $\hat{\alpha}$ being regarded as constant (rather than a function of κ) were used in the paper of Caulk and Naghdi (1978) and, with $\hat{\alpha}$ as a function of κ , are the same as those used by Naghdi and Nikkel (1984).

$$\begin{aligned}
g &= 4\mu^2 [\gamma_{KL} - (1 + \frac{\hat{\alpha}(\kappa)}{4\mu}) \gamma_{KL}^p] [\gamma_{KL} - (1 + \frac{\hat{\alpha}(\kappa)}{4\mu}) \gamma_{KL}^p] - \kappa \\
&= (\tau_{KL} - \frac{1}{2} \hat{\alpha}(\kappa) \gamma_{KL}^p) (\tau_{KL} - \frac{1}{2} \hat{\alpha}(\kappa) \gamma_{KL}^p) - \kappa = f
\end{aligned} \quad (2.2)$$

with

$$\hat{\alpha} = \hat{\alpha}(\kappa) = \frac{(\alpha_0 - \alpha_s)\kappa + \alpha_s \kappa_0 - \alpha_0 \kappa_s}{\kappa_0 - \kappa_s} \quad (2.3)$$

In (2.2) and (2.3) the coefficients $\alpha_0, \alpha_s, \kappa_0, \kappa_s$ are constants and μ is the elastic shear modulus. The constants α_0 and α_s are so chosen that $\hat{\alpha}(\kappa)$ takes the value α_0 when $\kappa = \kappa_0$ and takes the value α_s when $\kappa = \kappa_s$.

We adopt the loading criteria of strain space as primary. Then, after invoking the work assumption of Naghdi and Trapp (1975b), the constitutive equations for the rate of plastic strain \dot{e}_{KL}^p and the rate of work-hardening parameter $\dot{\kappa}$ may be expressed as (see the development among Eqs. (36)-(42) in Casey and Naghdi 1981):

$$\dot{e}_{KL}^p = \dot{\gamma}_{KL}^p = \begin{cases} 0, & \text{when } g < 0, \text{ or when } g = 0 \text{ and } \hat{g} \leq 0, \\ \frac{\hat{g}}{\Gamma + \Lambda} (2\tau_{KL} - \hat{\alpha} \gamma_{KL}^p), & \text{when } g = 0 \text{ and } \hat{g} > 0 \end{cases} \quad (2.4a,b)$$

and

$$\dot{\kappa} = (\hat{\beta}(\kappa) \tau_{KL} + \hat{\eta}(\kappa) \gamma_{KL}^p) \dot{e}_{KL}^p \quad (2.5)$$

In (2.4) and (2.5), the quantities $\hat{\beta}, \hat{\eta}$ are defined by

$$\hat{\beta} = \hat{\beta}(\kappa) = \left(\frac{\kappa - \kappa_s}{\kappa_0 - \kappa_s} \right) \beta, \quad \hat{\eta} = \hat{\eta}(\kappa) = \left(\frac{\kappa - \kappa_s}{\kappa_0 - \kappa_s} \right) \eta \quad (2.6)$$

β, η are constants,

$$\hat{g} = \frac{\partial g}{\partial e_{KL}} \dot{e}_{KL} = 4\mu (\tau_{KL} - \frac{1}{2} \hat{\alpha} \gamma_{KL}^p) \dot{\gamma}_{KL}^p \quad (2.7)$$

and on the yield surface $g = 0$,

$$\Lambda = 8\mu\kappa > 0 \quad (2.8)$$

$$\Gamma = 2\hat{\alpha}\kappa + 2[1 + \left(\frac{\alpha_0 - \alpha_s}{\kappa_0 - \kappa_s} \right) (\tau_{KL} - \frac{1}{2} \gamma_{KL}^p) \gamma_{KL}^p] (\hat{\beta} \tau_{MN} + \hat{\eta} \gamma_{MN}^p) (\tau_{MN} - \frac{1}{2} \gamma_{MN}^p) \quad (2.9)$$

The yield function f in (2.2) is of the von Mises type: it is quadratic in the deviatoric stresses and allows for translation and change in size of the yield surface. The amount of translation of the yield surface is linear in the deviatoric plastic strain and is also linear in κ through the coefficient α defined by (2.3). Also, the coefficient functions $\hat{\beta}(\kappa)$ and $\hat{\eta}(\kappa)$ which occur in (2.5) are linear in κ , they assume the respective values β and η at initial yield when $\kappa = \kappa_0$, and both vanish at saturation, i.e., when $\kappa = \kappa_s$, $\dot{\kappa} = 0$.

We also recall here that the strain-hardening behavior may be characterized by means of a rate-independent scalar quantity denoted here by ϕ (Casey and Naghdi, 1981, 1983)*. During loading the quantity ϕ has the same value as \hat{f}/\hat{g} , where $\hat{f} \equiv (\partial f / \partial s_{KL}) \dot{s}_{KL}$ and \hat{g} is defined by (2.7)₁. With the particular constitutive equations (i.e. generalized Hooke's law) used here and the work assumption of Naghdi and Trapp (1975b), ϕ can be expressed as

$$\phi = \frac{\Gamma}{\Gamma + \Lambda}, \quad (2.10)$$

and in fact since $\Gamma + \Lambda > 0$, Γ alone may be used to characterize the strain-hardening behavior (Casey and Naghdi 1984b, Eqs. (4.50) and (4.51)).

*It was demonstrated recently by Casey and Naghdi (1984a, Eq. (3.8)) that the quantity ϕ is equal to the determinant of a certain rate-independent fourth-order tensor which plays a fundamental role in the theory of plasticity and which arises naturally in relating the time rate of stress to the time rate of strain.

3. Equations for a Two-Dimensional State of Stress

Consider now the homogeneous deformation of an elastic-plastic material sustained by a biaxial state of stress (one normal component and one shearing component) in which the corresponding two components of strain are prescribed functions of time. Lamba and Sidebottom (1978a,b) modelled this experimentally by performing a strain-controlled combined tension-torsion test of a thin-walled circular cylinder in which the axial strain and the shear strain were prescribed functions of time. With the notation $s_{11}(t)$ for the axial stress and $s_{12}(t)$ for the shear stress, the two-dimensional state of stress can be represented in matrix notation as

$$\| \tau_{KL} \| = \frac{1}{3} s_{11} \| b_{KL} \| + s_{12} \| a_{KL} \| \quad , \quad \bar{s} = \frac{1}{3} s_{11} \quad , \quad (3.1)$$

where the constant matrices a_{KL} and b_{KL} defined by

$$\| a_{KL} \| = \begin{bmatrix} 0 & 1 & 0 \\ 1 & 0 & 0 \\ 0 & 0 & 0 \end{bmatrix} \quad , \quad \| b_{KL} \| = \begin{bmatrix} 2 & 0 & 0 \\ 0 & -1 & 0 \\ 0 & 0 & -1 \end{bmatrix} \quad (3.2)$$

are introduced for convenience.

The intended calculations require prescribing e_{11} and e_{12} parametrically as particular functions of time (which specify a path in the e_{11} - e_{12} plane), while the other two components of normal strain (e_{22} and e_{33}) remain so far unspecified and hence unknowns. Since $\dot{e}_{22}^p = \dot{e}_{33}^p = -\frac{1}{2} \dot{e}_{11}^p$ and $\dot{e}_{13}^p = \dot{e}_{23}^p = 0$ by (2.4) and (3.1), it follows that the plastic strain tensor can be expressed in the form

$$\| e_{KL}^p \| = \| \gamma_{KL}^p \| = \frac{1}{2} e_{11}^p \| b_{KL} \| + e_{12}^p \| a_{KL} \| \quad , \quad (3.3)$$

where e_{11}^p and e_{12}^p depend only on time. From the stress response (generalized Hooke's law) we have

$$s_{11} = E(e_{11} - e_{11}^p) \quad , \quad s_{12} = 2\mu(e_{12} - e_{12}^p) \quad , \quad (3.4)$$

where E is Young's modulus. From the inverted form of the stress response, as well as (3.3) and (3.4)₁, and after adopting the notation $e_r \equiv e_{22} = e_{33}$ we obtain

$$\|e_{KL}\| = \begin{vmatrix} e_{11} & e_{12} & 0 \\ e_{12} & e_r & 0 \\ 0 & 0 & e_r \end{vmatrix} \quad (3.5)$$

where

$$e_r = -\frac{\nu}{E} s_{11} - \frac{1}{2} e_{11}^p = -\nu e_{11} - \frac{1}{2}(1-2\nu)e_{11}^p \quad (3.6)$$

and where $\nu = (E-2\mu)/2\mu$ is Poisson's ratio. Equation (3.6) relates the unspecified components of strain to the axial strain (which is known) and the axial component of plastic strain. But e_r is still unknown, inasmuch as e_{11}^p remains unknown until all of the constitutive equations pertaining to a particular two-dimensional strain path have been integrated.

In order to simplify some of the expressions that follow, we introduce the abbreviations

$$M = s_{11} - \frac{3}{4} \hat{\alpha}(\kappa) e_{11}^p, \quad N = s_{12} - \frac{1}{2} \hat{\alpha}(\kappa) e_{12}^p. \quad (3.7)$$

Then, with the use of (3.1) to (3.6), the loading functions in (2.2) now assume the simplified forms

$$\begin{aligned} g &= \frac{2}{3} E^2 [e_{11} - (1 + \frac{3}{4} \frac{\hat{\alpha}}{E}) e_{11}^p]^2 + 8\mu^2 [e_{12} - (1 + \frac{\hat{\alpha}}{4\mu}) e_{12}^p]^2 - \kappa, \\ f &= \frac{2}{3} M^2 + 2N^2 - \kappa. \end{aligned} \quad (3.8)$$

For the two-dimensional state of stress defined by (3.1), Λ is still given by (2.8); but, on the yield surface, Γ in (2.9) now assumes the special form

$$\Gamma = 2\hat{\alpha}\kappa + \frac{4}{3} [1 + (\frac{\alpha_0 - \alpha_s}{\kappa_0 - \kappa_s}) (M e_{11}^p + 2N e_{12}^p)] [M (\beta s_{11} + \frac{3}{2} \hat{\alpha} e_{11}^p) + 3N (\beta s_{12} + \hat{\alpha} e_{12}^p)]. \quad (3.9)$$

In view of (3.1), (3.3), and (3.5), from (2.7) the quantity \hat{g} occurring in the loading criteria in strain space is given by

$$\begin{aligned}\hat{g} &= \frac{8}{3}\mu \dot{M}\dot{e}_{11} + 8\mu N\dot{e}_{12} - \frac{8}{3}\mu \dot{M}\dot{e}_r \\ &= \frac{4}{3}E\dot{M}\dot{e}_{11} + 8\mu N\dot{e}_{12} + \frac{4}{3}(3\mu - E)\dot{M}\dot{e}_{11}^p,\end{aligned}\quad (3.10a,b)$$

and the corresponding quantity \hat{f} in stress space is

$$\hat{f} = \frac{4}{3}M\dot{s}_{11} + 4N\dot{s}_{12}, \quad (3.11)$$

where in obtaining (3.10b) the time derivative of (3.6) has been used. It should be noted that \hat{g} depends on the unspecified strain rate \dot{e}_r (or the unknown axial plastic strain rate \dot{e}_{11}^p); and hence the determination of whether the state of strain at an elastic-plastic state is undergoing loading, neutral loading, or unloading cannot in general be ascertained directly from (3.10).

Since during loading the constitutive equation (2.4b) for the plastic strain rate contains \hat{g} on its right-hand side, in view of (3.10b) it is at once obvious that \dot{e}_{11}^p occurs on both sides of the equation in the case of axial plastic strain rate. After solving this equation, a new form of the constitutive equation results which depends only on the specified strain rates \dot{e}_{11} and \dot{e}_{12} . This equation then enables the constitutive equations for the other components of plastic strain rate to be expressed in terms of only \dot{e}_{11} and \dot{e}_{12} also. This procedure along with (3.1) and (3.3) leads to the following expressions for the non-zero plastic strain rates during loading ($g=0$, $\hat{g} > 0$)

$$\dot{e}_{11}^p = \frac{4}{3} \frac{M}{Q} \tilde{g}, \quad \dot{e}_{12}^p = \frac{2N}{Q} \tilde{g}, \quad \dot{e}_{22}^p = \dot{e}_{33}^p = -\frac{1}{2} \dot{e}_{11}^p, \quad (3.12)$$

where we have introduced the quantities Q and \tilde{g} defined by

$$Q = \Gamma + \Lambda - \frac{16}{9}(3\mu - E)M^2 \quad (3.13)$$

and

$$\tilde{g} = \hat{g} - \frac{4}{3}(3\mu - E)M\dot{e}_{11}^p = \frac{4}{3}EM\dot{e}_{11} + 8\mu N\dot{e}_{12} \quad (3.14)$$

It is shown in Appendix A under the assumption that $Q > 0$ always, which represents a range of strain-hardening behavior sufficiently general for our present purposes, that a knowledge of only the prescribed strain rates \dot{e}_{11} and \dot{e}_{12} is sufficient to determine whether the material at an elastic-plastic state is undergoing loading, neutral loading, or unloading. In fact, with $Q > 0$ the quantity \tilde{g} may be used in special loading criteria appropriate for the particular problem under discussion. Thus, with $Q > 0$, the constitutive equations for the plastic strain rate and the rate of work-hardening may alternatively be expressed as[†]

$$\dot{e}_{KL}^p = \begin{cases} 0 & , \text{ if } g < 0, & (a) \\ 0 & , \text{ if } g = 0 \text{ and } \tilde{g} < 0, & (b) \\ 0 & , \text{ if } g = 0 \text{ and } \tilde{g} = 0, & (c) \\ \text{Eq. (3.12)}, & \text{ if } g = 0 \text{ and } \tilde{g} > 0, & (d) \end{cases} \quad (3.15)$$

and

$$\dot{\kappa} = (\hat{\beta}s_{11} + \frac{3}{2}\hat{n}e_{11}^p)\dot{e}_{11}^p + 2(\hat{\beta}s_{12} + \hat{n}e_{12}^p)\dot{e}_{12}^p \quad (3.16)$$

where the loading criteria in (3.15a,b,c,d) correspond, respectively, to an elastic state, unloading from an elastic-plastic state, neutral loading at an elastic-plastic state, and loading at an elastic-plastic state.

We note that during unloading and neutral loading it follows from (2.4a), (3.4), (3.10b) and (3.11) that $\tilde{g} = \hat{g} = \hat{f}$, while during loading from (3.4) and (3.11) to (3.14) we have

$$\hat{f} = \frac{\Gamma}{Q}\tilde{g} = \frac{\Gamma}{\Gamma + \Lambda}\hat{g} \quad , (g=0, \hat{g} > 0) \quad (3.17)$$

[†]We emphasize that the loading criteria in (3.15) derived from the general form of the strain space loading criteria, and not postulated in an ad hoc fashion.

Results from the general theory similar to these and those obtained in Appendix A are summarized in Table 1 of Casey and Naghdi (1984c).

Before closing this section, we need to comment further on the restriction $Q > 0$ which bears on the loading criteria in (3.15). With reference to (3.13), since Γ may be used to characterize the strain-hardening behavior, with (2.8) and (3.8) the condition $Q > 0$ may be seen to include hardening behavior ($\phi > 0$) and perfectly plastic behavior ($\phi = 0$), but at first sight may appear to exclude a small range of softening behavior.⁵ However, it can be shown (Appendix A) that at an elastic-plastic state with $Q < 0$, the applied strain rates $\dot{\epsilon}_{11}$ and $\dot{\epsilon}_{12}$ can only be such that $\dot{g} < 0$. But the expression (3.14)₂ which occurs in the loading criteria (3.15) must be capable of admitting all possible choices of $\dot{\epsilon}_{11}$ and $\dot{\epsilon}_{12}$ (and hence capable of taking both positive and negative values) for all physically realistic tests. Since a state corresponding to $Q < 0$ is unnecessarily restrictive, it will be excluded from consideration in the present development.

⁵This is because the condition $Q > 0$ places a greater restriction on Γ than does the more general result $\Gamma + \Lambda > 0$ (which is a consequence of the work assumption of Naghdi and Trapp, 1975b).

4. Determination of Material Constants. Details of Calculations.

Previously a procedure was suggested for determining the material coefficients in the constitutive equations from the experimental data in a uniaxial cyclic loading test (Naghdi and Nikkel, 1984). This procedure is by no means unique; and, in fact, for data obtained from one-dimensional tests, other than uniaxial cyclic tests, it may be desirable to use a different procedure. Such alternative procedures are likely to be more advantageous in two or three dimensional tests. With reference to their experimental results for OFHC copper, Lamba and Sidebottom (1978a) note that the peak axial stress attained after the material has been cycled along a strain path such as that in Fig. 1(a) is significantly higher than the peak axial stress attained after simple uniaxial cycling. They go on to state that this difference indicates that "... material properties obtained from tensile tests or even uniaxial cyclic tests will not give accurate predictions of cyclic deformation under nonproportional or out-of-phase conditions."* A conclusion of this kind cannot be made independent of a particular theory used and does not follow from the knowledge of only a part of the experimental measurements (e.g., a part of the measurements that leads to the calculated s_{11}). Rather, it requires a detailed examination of the entire experimental data in conjunction with the relevant constitutive equations.

As can be seen from $(3.7)_{1,2}$ and $(3.8)_2$ with $\kappa = \kappa_s$, $\hat{\alpha}(\kappa) = \alpha_s$ and with $f=0$, the expression for κ_s in a two-dimensional cycling test depends on s_{11} , s_{12} , e_{11}^p , e_{12}^p as well as $\hat{\alpha} = \alpha_s$. However, the expression for κ_s in the case of a "peak" axial stress (i.e., the value of s_{11} when $s_{12} = 0$) will depend only on the axial stress s_{11} in addition to other parameters such as α_s and the

*The term out-of-phase refers to the specification of e_{11} and e_{12} as sinusoidal functions of time with the 90 degree phase difference between them, resulting in an elliptic path in the e_{11} - e_{12} plane.

plastic strains. We further observe that in the biaxial tests under discussion the value of the parameter κ_s , which represents the size of the loading surface in two-dimensions, is particularly sensitive to the values of the stresses but much less so to the values of α_s and the plastic strains. In view of the experimental result of Lamba and Sidebottom (1978a) mentioned in the previous paragraph, if κ_s is determined from uniaxial cycling data alone, then the theoretical prediction for the two-dimensional cycling experiments may not be as accurate as when κ_s is determined from the entire experimental data of a two-dimensional strain cycling test.

We keep the foregoing discussion in mind when describing the alternative procedure for determining the material coefficients in the constitutive equations. A value for κ_s will be determined from two-dimensional strain cycling experiments. For our present purpose, it will suffice to determine the other constants from uniaxial cycling data as before.[†] Thus, a value for κ_0 follows from $f=0$ and the yield stress in uniaxial tension, and a value for α_s can be determined from the slope of the uniaxial stress strain curve at saturation. By selecting a point at saturation from the experimental data for a two-dimensional cycling experiment, similar to points Q, R, S or T shown in the calculated results in Figs. 1(a-c) and with the values of stress and plastic strain at such a point of value for κ_s may be determined from $f=0$. We took the value κ_s to be the average of the values obtained from points R and T, in order to have the best overall prediction for all loading paths in the e_{11} - e_{12} plane. The remaining constants may then be determined from the uniaxial cycling data by the procedure described previously (Naghdi and Nikkel, 1984). Using the above procedure with the experimental data of Lamba and Sidebottom (1978a, Figs. 2 and 3(a-d)) for OFHC copper the material constants were determined to

[†] In contrast to κ_s , for the relatively simple constitutive equations used here the determination of the other constants from the uniaxial tests seems to be adequate.

be

$$\begin{aligned} \frac{\alpha_0}{E} = \frac{\alpha_s}{E} &= 8.14 \times 10^{-3} \quad , \quad \frac{\beta}{E} = 2.30 \times 10^{-2} \quad , \quad \frac{\eta}{E^2} = -9.38 \times 10^{-5} \quad , \\ \frac{\kappa_0}{E^2} &= 4.03 \times 10^{-8} \quad , \quad \frac{\kappa_s}{E^2} = 1.93 \times 10^{-6} \quad , \quad \frac{\mu}{E} = 0.374 \quad , \\ E &= 115 \text{ GPa} \quad . \end{aligned} \tag{4.1}$$

In the course of identifying values for the coefficients α_0 and α_s , it was found that their values differed only by less than 0.3%. This suggests that if this difference can be neglected, we could set $\alpha_0 = \alpha_s$ approximately and then the coefficient η in (2.5) and (2.6) will no longer require an independent identification. This would make the task of determination of the coefficients much easier; and, in fact, with $\alpha_0 = \alpha_s$ the coefficient η can be determined in terms of α_0 and β . To see this, we recall that in the special case in which $\alpha_0 = \alpha_s \equiv \alpha$ (say) the constitutive equations used here reduce to a special case of those employed previously by Caulk and Naghdi (1978, Eqs. (40), (56) and (70)₁). For their equations, they obtained the restriction $\eta = -\frac{1}{2}\alpha\beta$ (see Eq. (70)₂ in Caulk and Naghdi, 1978). In view of the fact that the values determined for α_0 and α_s are essentially the same, for the purpose of comparison with the experimental data of Lamba and Sidebottom (1978a,b) for OFHC copper, it will suffice to take $\alpha_0 = \alpha_s$ and $\eta = -\frac{1}{2}\alpha_0\beta$.

The calculations summarized in Section 1 were carried out by first parametrically specifying the strains e_{11} and e_{12} as functions of time, corresponding to a particular path in the e_{11} - e_{12} plane. The constitutive equations (3.15) and (3.16) were then integrated numerically with the values (4.1) for the coefficients. Finally, the stresses were calculated using (3.4).

To calculate ϕ in (2.10), a knowledge of Λ in (2.8) and Γ in (3.9) is needed. The particular representation of Γ in (3.9) depends on the stresses,

as well as the quantities M and N which also involve the stresses s_{11} and s_{12} . Then, in view of (3.4), Γ may be expressed in terms of the total and plastic strains. It follows that ϕ depends on total and plastic strains, as well as on κ . But, from the fact that on the yield surface $g = 0$ with the function g given by (3.8)₁, it is possible to solve for κ in terms of the other quantities so that ϕ may be represented as a function of only e_{11} , e_{12} , e_{11}^p , and e_{12}^p . It is of interest to plot the variation of ϕ with plastic strains for fixed values of e_{11} and e_{12} . After making the substitutions indicated above, the dependence of ϕ on the total and plastic strains may be expressed in the form

$$\phi = \hat{\phi}(e_{11}^p - (1 + \frac{3}{4} \frac{\alpha_0}{E})^{-1} e_{11}, e_{12}^p - (1 + \frac{\alpha_0}{4\mu})^{-1} e_{12}). \quad (4.2)$$

For definiteness, we specify $e_{11} = e_{12} = 0$ and then calculate the value of ϕ for each e_{11}^p, e_{12}^p pair. The resulting plot using the values (4.1) is shown in Fig. 4. It is clear from the arguments of the function $\hat{\phi}$ in (4.2) that this single calculation provides all of the relevant information on the variation of ϕ ; and, for any other specified values of e_{11} and e_{12} , the surface plotted in Fig. 4 will not change in shape but will simply translate parallel to the $e_{11}^p - e_{12}^p$ plane by the constant amounts

$$(1 + \frac{3}{4} \frac{\alpha_0}{E})^{-1} e_{11}, \quad (1 + \frac{\alpha_0}{4\mu})^{-1} e_{12} \quad (4.3)$$

in the e_{11}^p and e_{12}^p directions respectively. It must be kept in mind that the domain in the $e_{11}^p - e_{12}^p$ plane must be such that the value of κ corresponding to the values of e_{11} , e_{12} , e_{11}^p and e_{12}^p is between κ_0 and κ_s . In Fig. 4 the outer boundary, with the smallest value of ϕ corresponds to $\kappa = \kappa_s$ and the inner boundary, with the largest value of ϕ corresponds to $\kappa = \kappa_0$. It should be mentioned that some elastic-plastic states corresponding to points on the surface

may not be reached by any path. For example, on the inner boundary in Fig. 4, where $\kappa = \kappa_0$, the plastic strain is nonzero indicating some plastic deformation must occur to reach an elastic-plastic state corresponding to this edge of the surface. However, after plastic deformation has taken place κ cannot have the value κ_0 (the value of κ at initial yield) while the material exhibits hardening behavior except in the special case of purely kinematic hardening. Thus, for the plot displayed in Fig. 4, no actual elastic-plastic state corresponding to the inner boundary of the surface can be reached.

5. Concluding Remarks

In summary, a relatively simple set of constitutive equations is used to predict various phenomena occurring in two-dimensional strain cycling in the range of small deformation. The calculated predictions are compared with corresponding experimental results of Lamba and Sidebottom (1978a,b) with good qualitative agreements. It is noteworthy that even during the post-saturation behaviour of the material, the constitutive equations used have adequate predictive capabilities as demonstrated by the results in Figs. (2(a-c)) and Figs. (3(a-c)). Also, it may be emphasized that the theoretical calculations successfully predict the erasure of memory phenomenon which has significant practical utility in two-dimensional, post-saturation strain cycling experiments. Clearly, by exploiting this phenomenon, the response of a material to strain cycling along strain paths in different directions can be determined by performing experiments on one specimen if a large cycle which erases the material's memory of the preceding smaller cycle is traversed after each smaller cycle.

The main differences between the present calculations and the experimental results can be attributed primarily to the manner of identification of two of the material constants at saturation, namely κ_s and α_s . These values can be chosen to be the same as those identified either from experiments in simple tension ($e_{12} = 0$) or experiments in simple shear ($e_{11} = 0$). The values resulting from experiments in simple tension can lead to discrepancies in matching experiments involving mainly simple shear (such as those in Figs. (2(a-c)) and (3(a-c))), and likewise values chosen from experiments in simple shear will affect the agreements between the theoretical and experimental results in simple tension. The choice for the value of the constant κ_s used in the calculations (for details see Sec. 4) was motivated by a desire to obtain the best overall agreement with experimental results for all directions of the strain paths in the e_{11} - e_{12} plane. Similarly, as noted in the last section, α_s was chosen to be equal to α_0 in order to simplify

the identification of the material coefficients for OFHC copper. The slope of the calculated response curve in the s_{12} - e_{12} plane at saturation can be shown to depend to some degree on α_s , so that if a more accurate prediction of the slope of the curve during loading along FB in Fig. 2(c) is desired an alternative procedure for determination of α_s could be used.*

The plot displayed in Fig. 4 contains detailed information pertaining to strain-hardening behaviour for the particular material used in the experiments of Lamba and Sidebottom (1978a,b). Accessibility to such information or the data representing ϕ for all values of total and plastic strains in the domain of interest is clearly of value in analyses and computations. It should be possible in principle to determine the value of ϕ directly from experiments. Casey and Naghdi (1984b, Eq. (4.29)) have previously shown that the function ϕ can be interpreted in terms of the ratio of the outward normal velocities of the yield surfaces in stress space and in strain space. It is suggested that future experimenters provide direct measurements concerning the yield surfaces in both stress space and strain space and also consider the possibility of obtaining the values of ϕ directly in the course of their experiments.

We close this section with some remarks concerning additional experimental data on two-dimensional cycling that have become available very recently.

*In addition to the two elastic constants, there are six material constants ($\alpha_0, \alpha_s, \beta, \eta, \kappa_0, \kappa_s$) which must be determined from experimental results. However, for the special case in which $\alpha_0 = \alpha_s$ as utilized in Section 4, an additional restriction obtained by Caulk and Naghdi (1978) can also be invoked and this reduces the number of independent constants to be determined to the four ($\alpha_0, \beta, \kappa_0, \kappa_s$). With $\alpha_0 \neq \alpha_s$, the calculations will involve more complex expressions and plots (for different values of e_{11}, e_{12}) of the function ϕ will exhibit changes in shape and will not simply represent translations of the surface parallel to the e_{11}^p - e_{12}^p plane as in the case when $\alpha_0 = \alpha_s$.

McDowell (1985) has reported experimental results for two-dimensional strain cycling of a type similar to those of Lamba and Sidebottom (1978a,b); and in principle, similar comparisons can be made with his data. However, the data provided in McDowell's paper are insufficient for the identification of all of the material constants appearing in the constitutive equations used here.[§] Also, it should be noted that our approach for theoretical predictions differs from the "two surface stress space model" used by McDowell (1985) for comparison with his experiments.

Ohashi et al. (1985) have reported some experimental data for two-dimensional stress cycling. They do not discuss any theoretical predictions for comparison with their experiments. While in principle, there should be no difficulty in making such comparisons, the data provided is again insufficient for the identification of all of the material constants appearing in the constitutive equations used here.[†]

Acknowledgement. The results reported here were obtained in the course of research supported by the Solid Mechanics Program of the U.S. Office of Naval Research under Contract N00014-84-K-0264, Project NR 064-436 with the University of California, Berkeley.

[§] McDowell's paper (1985) does not include the data for uniaxial strain cycling needed for the identification of material constants in the context of the procedure used here.

[†] Ohashi et al. (1985) do not perform any uniaxial strain cycling tests. The data from such tests are necessary for identification of most of the material constants using the procedure summarized in Sec. 4.

Appendix A

We include here the details of the arguments which demonstrate that the special loading criteria in (3.15) with \tilde{g} (rather than \hat{g}) are consistent with the loading criteria of the strain-space formulation, i.e., at an elastic-plastic state with $Q > 0$ we establish the correspondence

$$\begin{aligned}\tilde{g} < 0 &\Leftrightarrow \hat{g} < 0, & (\text{unloading}), \\ \tilde{g} = 0 &\Leftrightarrow \hat{g} = 0, & (\text{neutral loading}), \\ \tilde{g} > 0 &\Leftrightarrow \hat{g} > 0, & (\text{loading}).\end{aligned}$$

We first prove that at an elastic-plastic state with $Q \neq 0$, $\hat{g} = 0$ if and only if $\tilde{g} = 0$. Sufficiency follows from (3.12), where if $\tilde{g} = 0$ so is $\dot{e}_{KL}^p = 0$ and then from (3.14) $\hat{g} = 0$ also. To establish necessity suppose that $\hat{g} = 0$. It then follows from (2.4) and (3.14) that $\tilde{g} = 0$.

In view of the result of the previous paragraph note that at an elastic-plastic state with $Q \neq 0$, $\hat{g} \neq 0$ if and only if $\tilde{g} \neq 0$. We now prove that at an elastic-plastic state with $Q > 0$, $\hat{g} > 0$ if and only if $\tilde{g} > 0$. To establish sufficiency suppose that $\tilde{g} > 0$. If $\hat{g} < 0$, then $\dot{e}_{KL}^p = 0$ by (2.4) and (3.14) implies $\hat{g} = \tilde{g}$, which is a contradiction and hence we must have $\hat{g} > 0$. To establish necessity, we suppose that $\hat{g} > 0$, and this implies that $\hat{g} = \tilde{g}(\Gamma + \Lambda)/Q$ from (3.17). In view of the fact that $\Gamma + \Lambda > 0$ (Casey and Naghdi, 1984b, Eq. (4.50)) and the fact that we are considering only the case in which $Q > 0$ this implies $\tilde{g} > 0$.

As a consequence of the results of the preceding two paragraphs, it follows that at an elastic-plastic state with $Q > 0$, $\hat{g} < 0$ if and only if $\tilde{g} < 0$.

In the remainder of this appendix we demonstrate that if Q in (3.13) is

nonpositive at an elastic-plastic state, i.e., if $Q \leq 0$, then the applied strain rates $\dot{\epsilon}_{11}$ and $\dot{\epsilon}_{12}$ can only be such that $\tilde{g} \leq 0$.

We first prove that with $Q < 0$ we can only have $\tilde{g} \leq 0$. Suppose $\tilde{g} > 0$. If $\hat{g} \leq 0$, then (2.4) and (3.14) imply $\tilde{g} = \hat{g}$ which is a contradiction. Alternatively if $\hat{g} > 0$, then $\hat{g} = \tilde{g}(\Gamma + \Lambda)/Q$ from (3.17). In view of the fact that $\Gamma + \Lambda > 0$ (Casey and Naghdi, 1984b, Eq. (4.50)) and that we are considering the case in which $Q < 0$, it follows that $\tilde{g} < 0$ which is also a contradiction. Hence, we can only have $\tilde{g} \leq 0$ if $Q < 0$.

Next, we prove that if $Q=0$, we can only have $\tilde{g} \leq 0$. Again, suppose that $\tilde{g} > 0$. If $\hat{g} \leq 0$, then (2.4) and (3.14) imply $\tilde{g} = \hat{g}$ which is a contradiction. Alternatively, if $\hat{g} > 0$, with the use of the expression for \hat{g} resulting from (3.14)₁ and the identity resulting from (3.13) after setting its left-hand side equal to zero, the constitutive equation for the axial plastic strain rate from (2.4b) implies $\tilde{g} = 0$ which is also a contradiction. Hence we can only have $\tilde{g} \leq 0$ if $Q = 0$.

References

- Casey, J., and Lin, H. H., 1983, "Strain-Hardening Topography of Elastic-Plastic Materials," ASME Journal of Applied Mechanics, Vol. 50, pp. 795-801.
- Casey, J., and Naghdi, P. M., 1981, "On the Characterization of Strain-Hardening in Plasticity," ASME Journal of Applied Mechanics, Vol. 48, pp. 285-296.
- Casey, J., and Naghdi, P. M., 1983, "A Remark on the Definition of Hardening, Softening and Perfectly Plastic Behavior," Acta Mechanica, Vol. 48, pp. 91-94.
- Casey, J., and Naghdi, P. M., 1984a, "Further Constitutive Results in Finite Plasticity," Quarterly Journal of Mechanics and Applied Mathematics, Vol. 37, pp. 231-259.
- Casey, J., and Naghdi, P. M., 1984b, "Strain-Hardening Response of Elastic-Plastic Materials," presented at a Conference on "Constitutive Laws for Engineering Materials: Theory and Application," Tuscon, AZ., January 10-14, 1983. In Mechanics of Engineering Materials, edited by C. S. Desai and R. H. Gallagher, Chapt. 4, John Wiley & Sons Ltd.
- Casey, J., and Naghdi, P. M., 1984c, "Constitutive Results for Finitely Deforming Elastic-Plastic Materials," in Constitutive Equations: Macro and Computational Aspects, William, K. J., ed., The American Society of Mechanical Engineers, New York, pp. 53-71.
- Caulk, D. A., and Naghdi, P. M., 1978, "On the Hardening Response in Small Deformation of Metals," ASME Journal of Applied Mechanics, Vol. 45, pp. 755-764.
- Green, A. E., and Naghdi, P. M., 1965, "A General Theory of an Elastic-Plastic Continuum," Archive for Rational Mechanics and Analysis, Vol. 18, pp. 251-281.
- Green, A. E., and Naghdi, P. M., 1966, "A Thermodynamic Development of Elastic-Plastic Continua," Proceedings of the IUTAM Symposium on Irreversible Aspects of Continuum Mechanics and Transfer of Physical Characteristics in Moving Fluids, Parkus, H., and Sedov, L. I., eds., Springer-Verlag, New York, pp. 117-131.
- Lamba, H. S., and Sidebottom, O. M., 1978a, "Cyclic Plasticity for Nonproportional Paths: Part 1 - Cyclic Hardening, Erasure of Memory, and Subsequent Strain Hardening Experiments," ASME Journal of Engineering Materials and Technology, Vol. 100, pp. 96-103.
- Lamba, H. S., and Sidebottom, O. M., 1978b, "Cyclic Plasticity for Nonproportional Paths: Part 2 - Comparison With Predictions of Three Incremental Plasticity Models," ASME Journal of Engineering Materials and Technology, Vol. 100, pp. 104-111.

- McDowell, D. L., 1985, "A Two Surface Model for Transient Nonproportional Cyclic Plasticity; Part 2 Comparison of Theory with Experiments," ASME Journal of Applied Mechanics, Vol. 52, pp. 303-308.
- Naghdi, P. M. and Nikkel, D. J., Jr., 1984, "Calculations for Uniaxial Stress and Strain Cycling in Plasticity," ASME Journal of Applied Mechanics, Vol. 51, pp. 487-493.
- Naghdi, P. M., and Trapp, J. A., 1975a, "The Significance of Formulating Plasticity Theory With Reference to Loading Surfaces in Strain Space," International Journal of Engineering Science, Vol. 13, pp. 785-797.
- Naghdi, P. M., and Trapp, J. A., 1975b, "Restrictions on Constitutive Equations of Finitely Deformed Elastic-Plastic Materials," Quarterly Journal of Mechanics and Applied Mathematics, Vol. 28, pp. 25-46.
- Ohashi, Y., Kawai, M., and Kaito, T., 1985, "Inelastic Behavior of Type 316 Stainless Steel Under Multiaxial Nonproportional Cyclic Stressings at Elevated Temperature," ASME Journal of Engineering Materials and Technology, Vol. 107, pp. 101-109.

Captions for Figures

Fig. 1(a) Comparison of the stress trajectory in s_{11} - s_{12} plane (measured in MPa) between the theoretical prediction (—) and the experimental data (- - -) from Lamba and Sidebottom (1978a) for OFHC copper; the numerical calculation of the theoretical trajectory was effected with the use of (3.4), (3.15), (3.16) and the constants (4.1). The prescribed strain path in the e_{11} - e_{12} plane is shown in the inset. After initial elongation from the undeformed state to point Q, the nearly elliptical path QRSTQ is repeatedly traversed. While the path in the e_{11} - e_{12} plane is cyclic, the remaining nonzero components of strain do not necessarily return to the same values at the end of each cycle. Comparison with the experimental data is shown for the first few cycles only, since the portion of the trajectory for additional cycles would crowd the figure.

Fig. 1(b) Comparison of the theoretical (—) axial stress response, measured in MPa, with the corresponding experimental data (- - -) of Lamba and Sidebottom (1978a) for OFHC copper according to the prescribed strain path in the inset of Fig. 1(a). Comparison with the experimental data is shown for the first few cycles only, since the portion of the curve for additional cycles would crowd the figure.

Captions for Figures (continued)

- Fig. 1(c) Comparison of the theoretical (—) shear stress response, measured in MPa, with the corresponding experimental data (- - -) of Lamba and Sidebottom (1978a) for OFHC copper according to the prescribed strain path in the inset of Fig. 1(a). Comparison with the experimental data is shown for the first few cycles only, since the portion of the curve for additional cycles would crowd the figures.
- Fig. 2(a) The theoretical stress trajectory in s_{11} - s_{12} plane (measured in MPa) calculated from (3.4), (3.15) and (3.16) for OFHC copper using the constants (4.1). The prescribed strain path in the e_{11} - e_{12} plane is shown in the inset. Calculation for a state of saturation was obtained by first cycling in shear along B'D'B' in the e_{11} - e_{12} plane for four cycles followed by cycling along the elliptical path B'CD'EB' for four cycles. After this saturation was attained, the smaller path BDBFB was repeatedly traversed. Only the portion of the stress trajectory which corresponds to the (post saturation) strain path BDBFB is shown.
- Fig. 2(b) Comparison of the theoretical (—) axial stress response, measured in MPa, with the corresponding experimental data (- - -) of Lamba and Sidebottom (1978a) for OFHC copper according to the prescribed strain path in the inset of Fig. 2(a). Only the portion of the stress response which corresponds to the (post saturation) strain path BDBFB is shown.

Captions for Figures (continued)

- Fig. 2(c) Comparison of the theoretical (—) shear stress response, measured in MPa, with the corresponding experimental data (- - -) of Lamba and Sidebottom (1978a) for OFHC copper according to the prescribed strain path in the inset of Fig. 2(a). Only the portion of the stress response which corresponds to the (post saturation) strain path BDBFB is shown.
- Fig. 3(a) Comparison of the stress trajectory in s_{11} - s_{12} plane (measured in MPa) between the theoretical prediction (—) and the experimental data (- - -) from Lamba and Sidebottom (1978b) for OFHC copper; the numerical calculation of the theoretical trajectory was effected with the use of (3.4), (3.15), (3.16) and the constants (4.1). The prescribed strain path in the e_{11} - e_{12} plane is shown in the inset. Calculation for a state of saturation was obtained in a similar manner to that in Fig. 2(a). After the saturation was attained, the complex path 0-1, 1-2, ..., 7-8 was repeatedly traversed. Only the portion of the stress trajectory which corresponds to the (post saturation) strain path 0-8 is shown.
- Fig. 3(b) Comparison of the theoretical (—) axial stress response, measured in MPa, with the corresponding experimental data (- - -) of Lamba and Sidebottom (1978b) for OFHC copper according to the prescribed strain path in the inset of Fig. 3(a). Only the portion of the stress response which corresponds to the (post saturation) strain path 0-8 is shown.

Captions for Figures (continued)

Fig. 3(c) Comparison of the theoretical (—) shear stress response, measured in MPa, with the corresponding experimental data (- - -) of Lamba and Sidebottom (1978b) for OFHC copper according to the prescribed strain path in the inset of Fig. 3(a). Only the portion of the stress response which corresponds to the (post saturation) strain path 0-8 is shown.

Fig. 4 A geometrical representation of the function ϕ (which characterizes strain-hardening) as a surface exhibiting its dependence on the plastic strain components e_{11}^p and e_{12}^p , plotted for fixed values of the total strains (in this figure taken to be $e_{11}=e_{12}=0$) for OFHC copper having the material constants specified in (4.1). For different values of e_{11} and e_{12} , the surface merely translates parallel to the plane of (e_{11}^p, e_{12}^p) but does not change its shape. An example of how the value of ϕ may be determined from this plot is also indicated: At a typical point on the surface, the values of the plastic strains e_{11}^p, e_{12}^p are known (the coordinate curves on the surface are drawn at plastic strain intervals of 0.0002) and the corresponding point in the e_{11}^p - e_{12}^p plane is located. Then, the value of ϕ is measured by comparing the vertical distance between the point on the plane and the point on the surface with the scale on the ϕ axis.

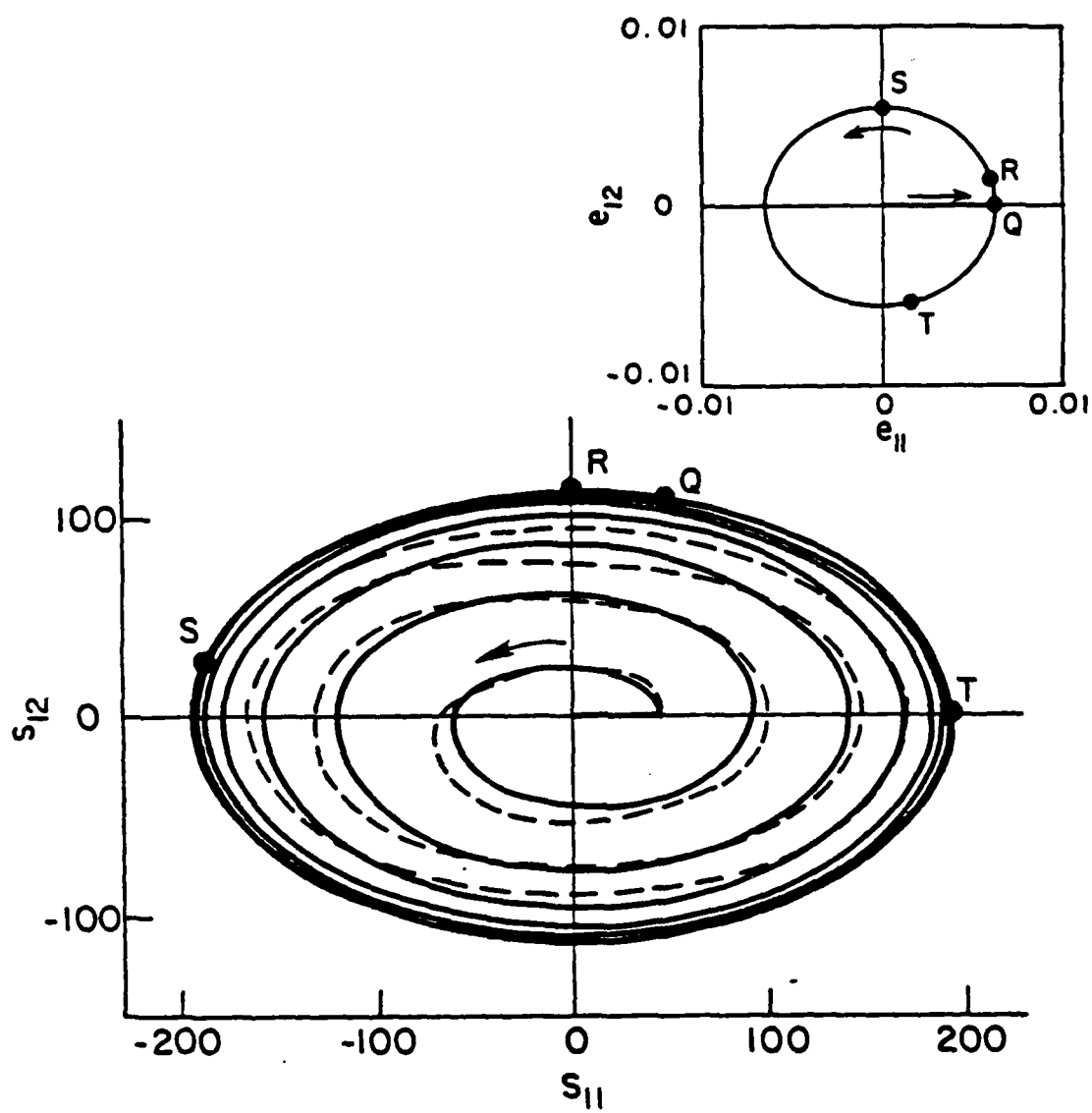


Fig. 1(a)

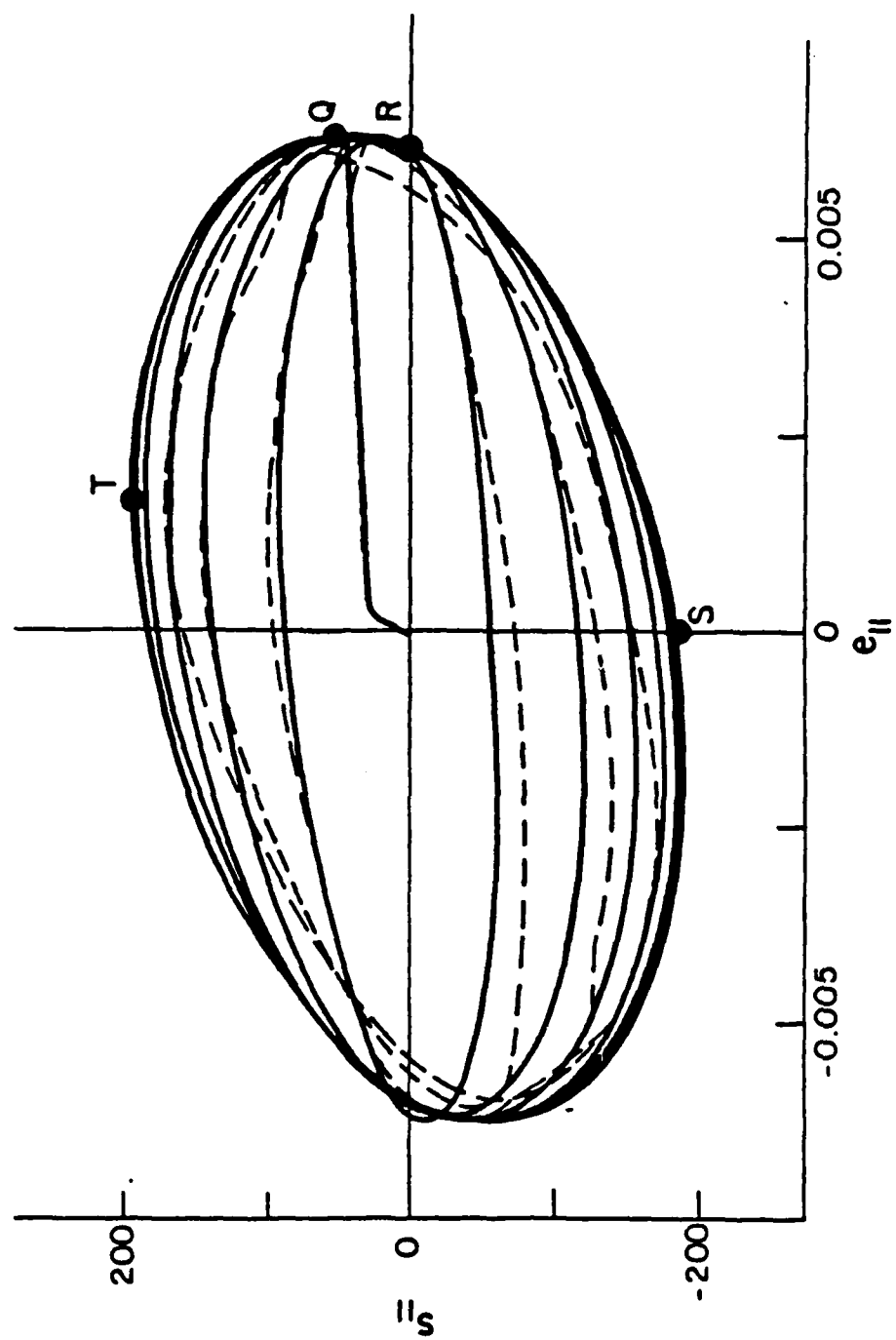


Fig. 1(b)

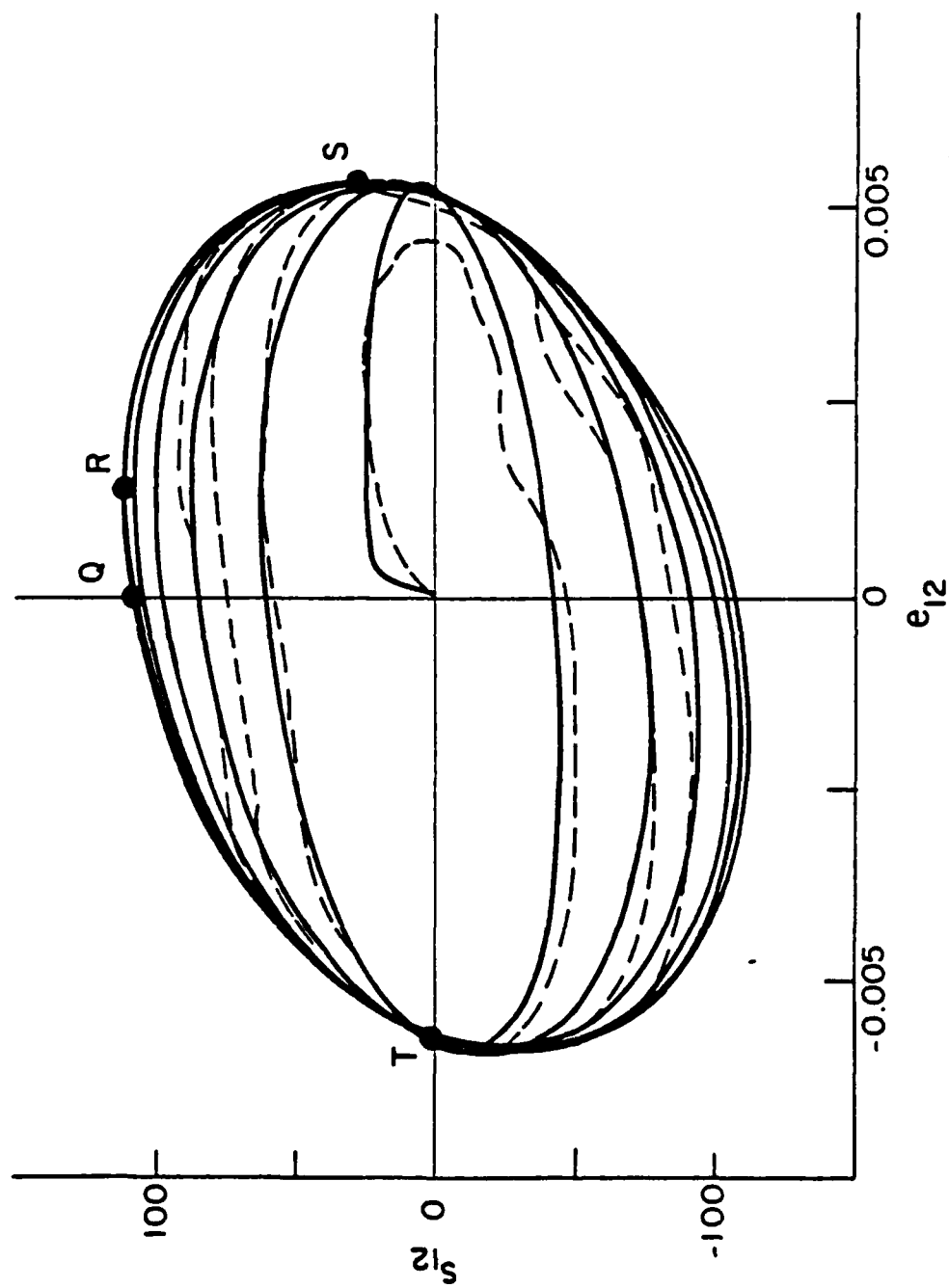


Fig. 1(c)

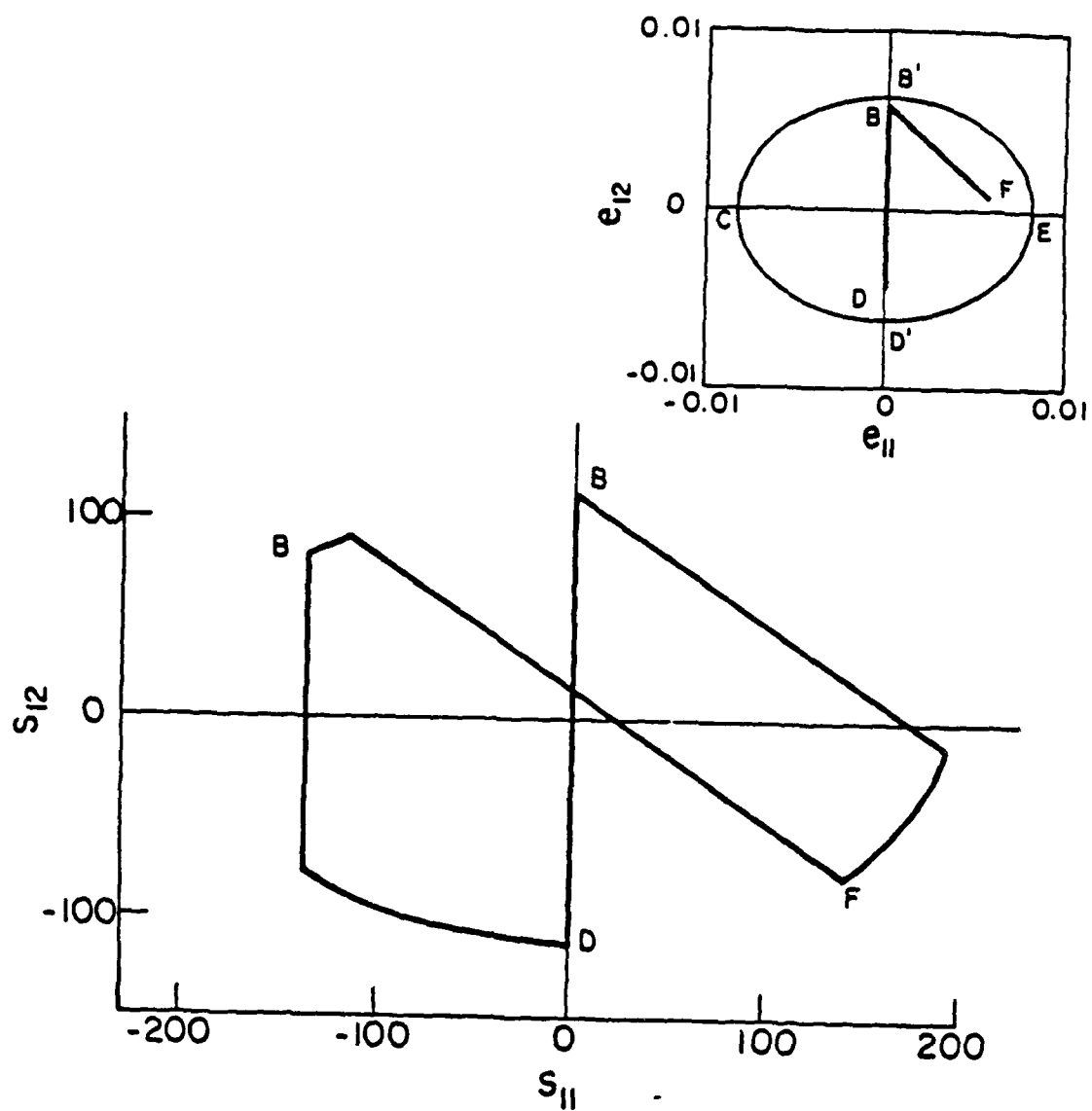


Fig. 2(a)

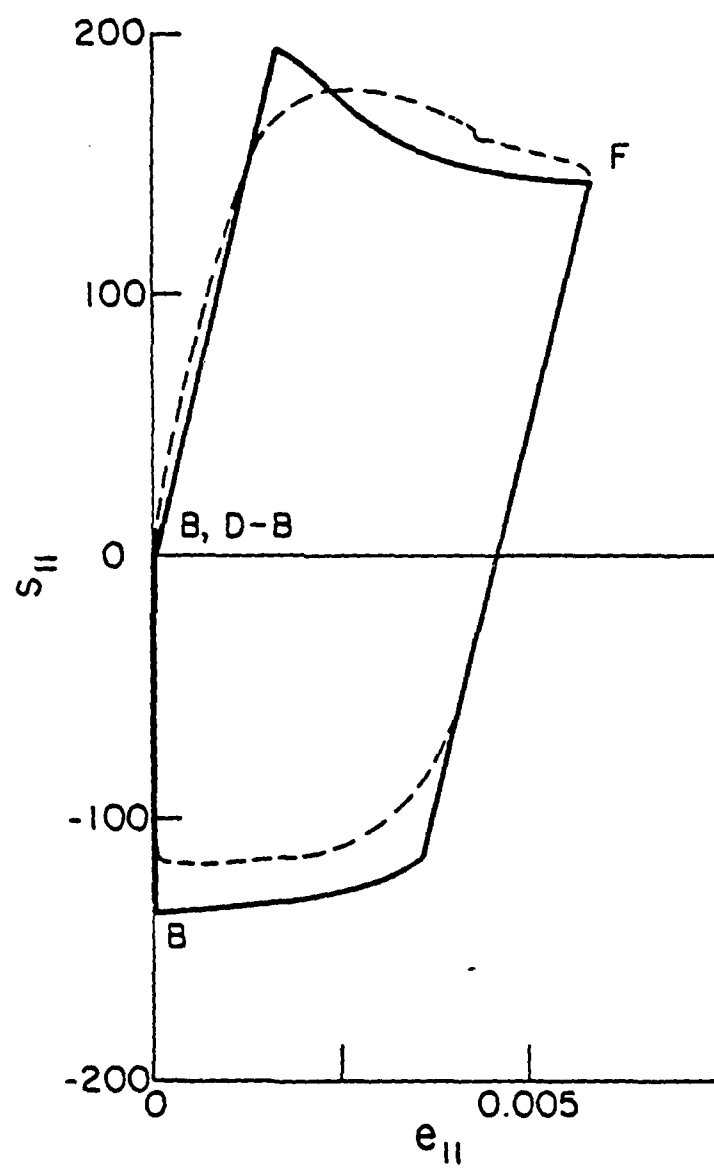


Fig. 2(b)

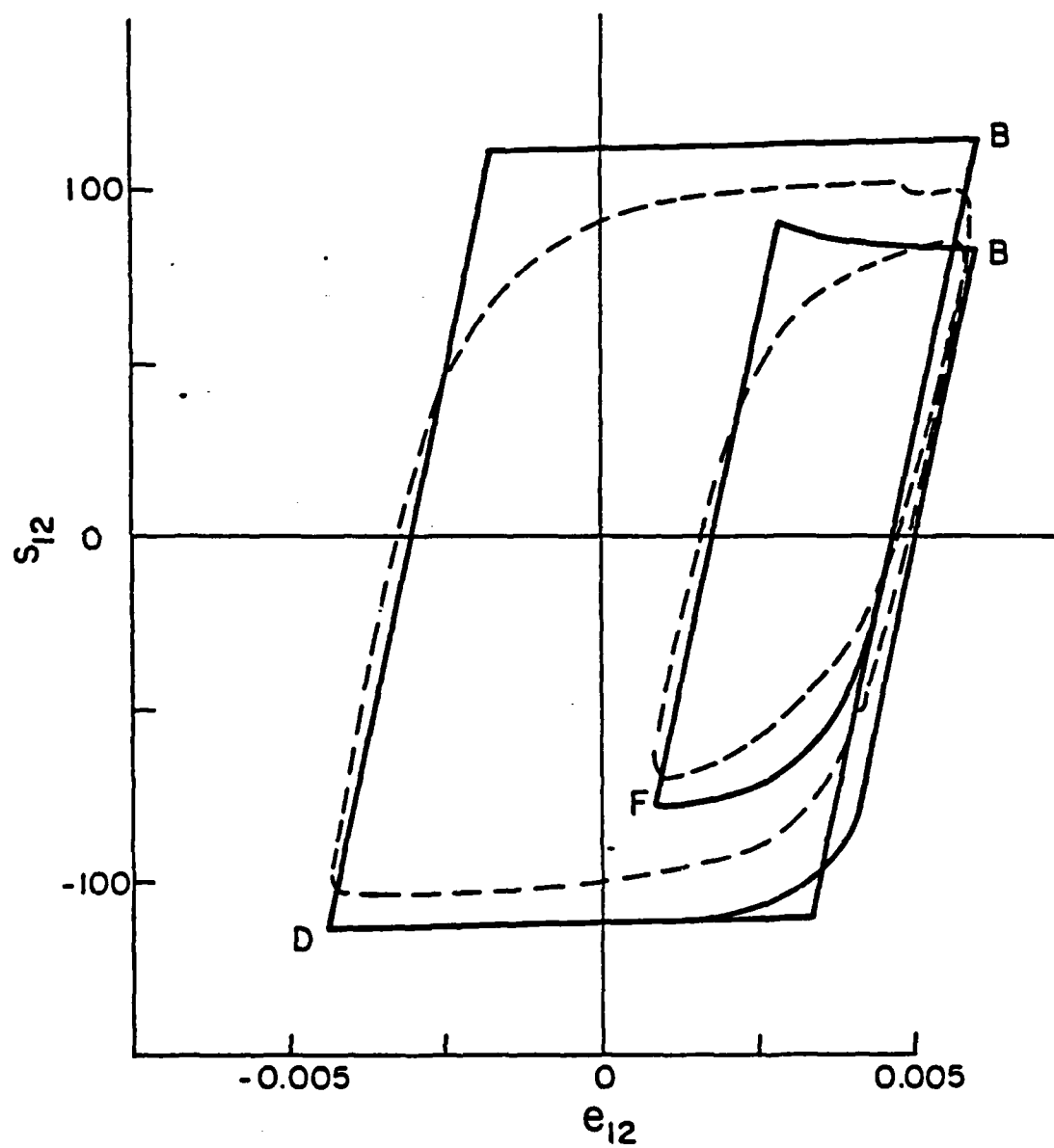


Fig. 2(c)

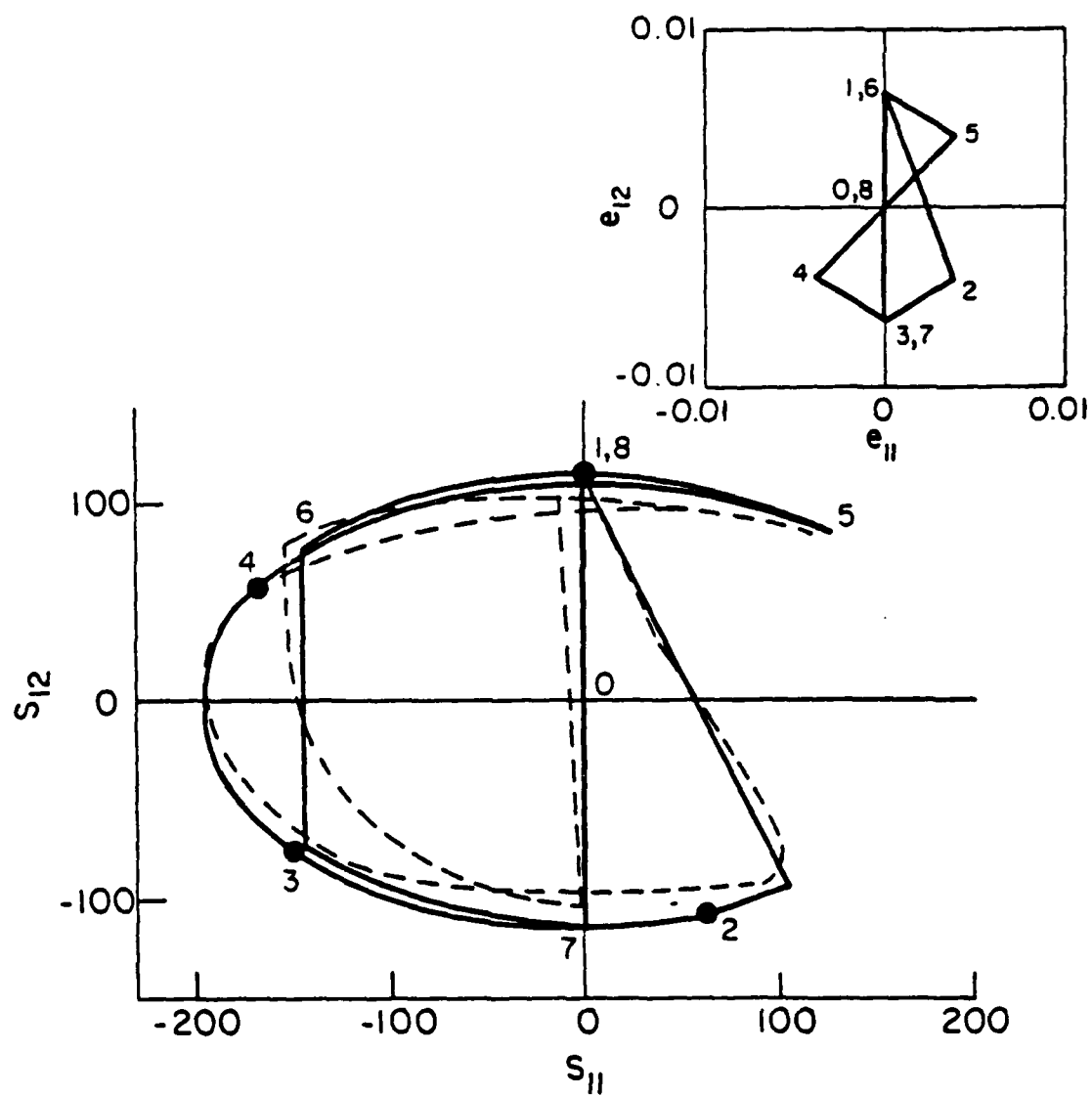


Fig. 3(a)

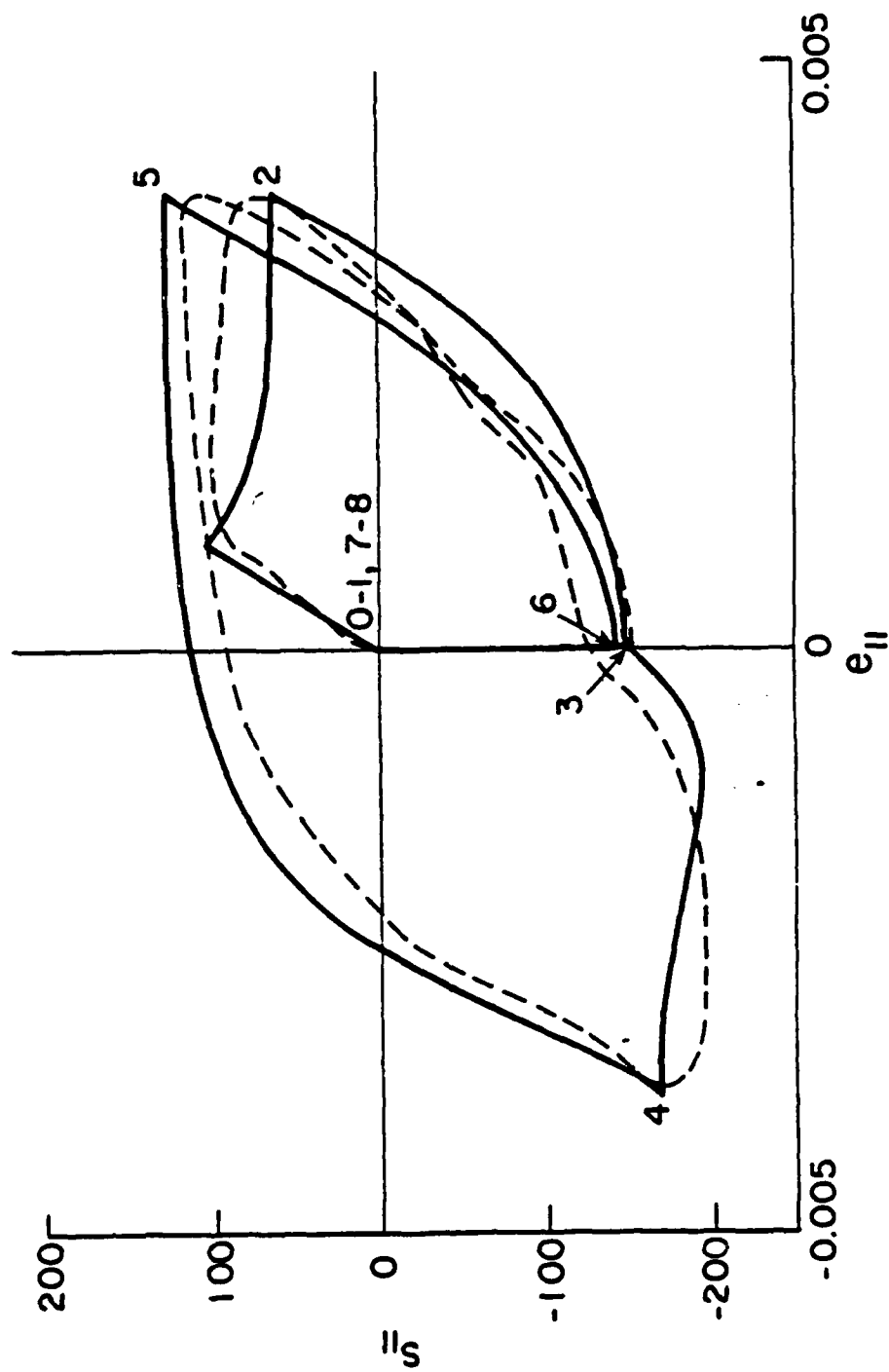


Fig. 3(b)

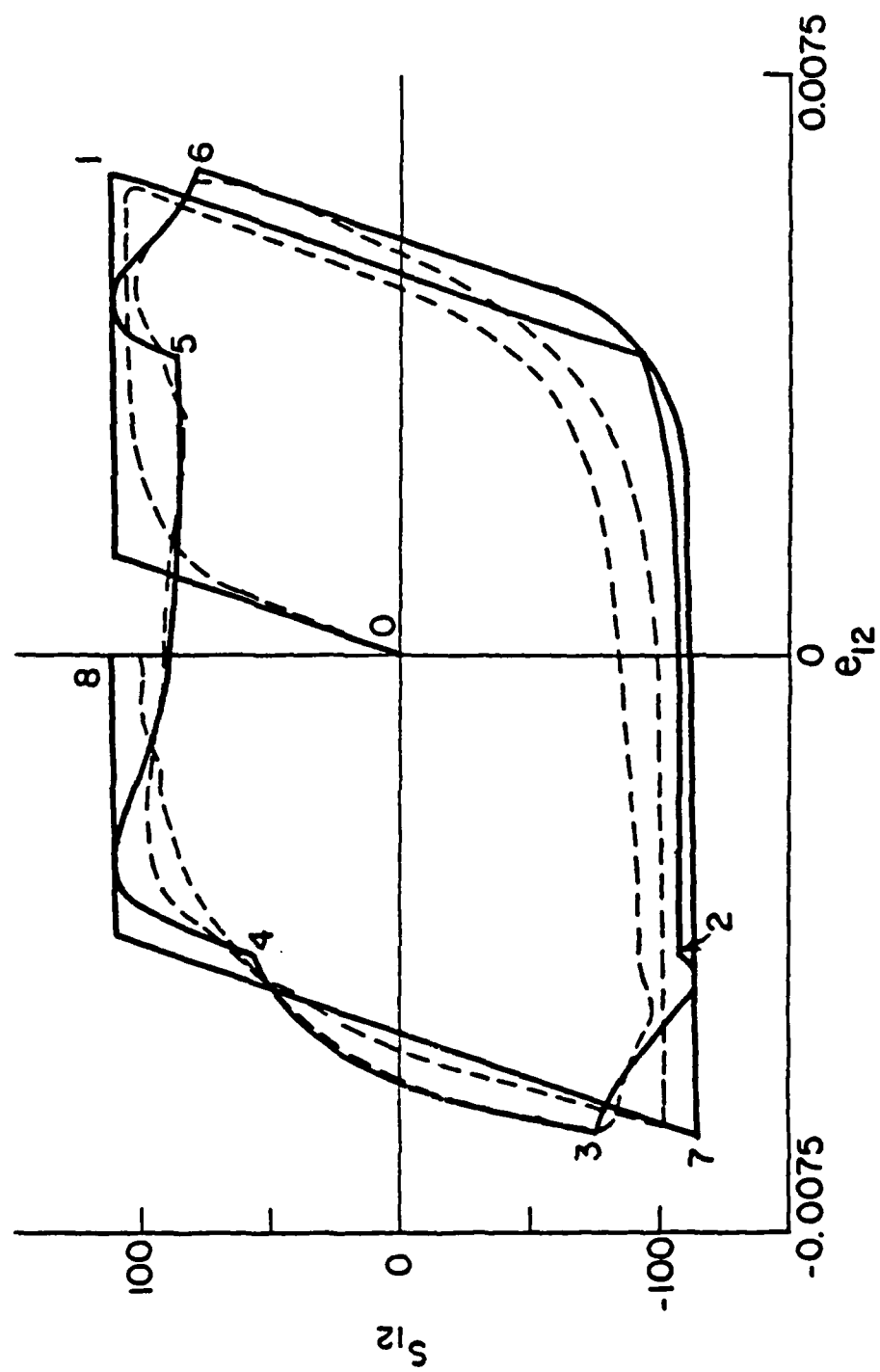


Fig. 3(c)

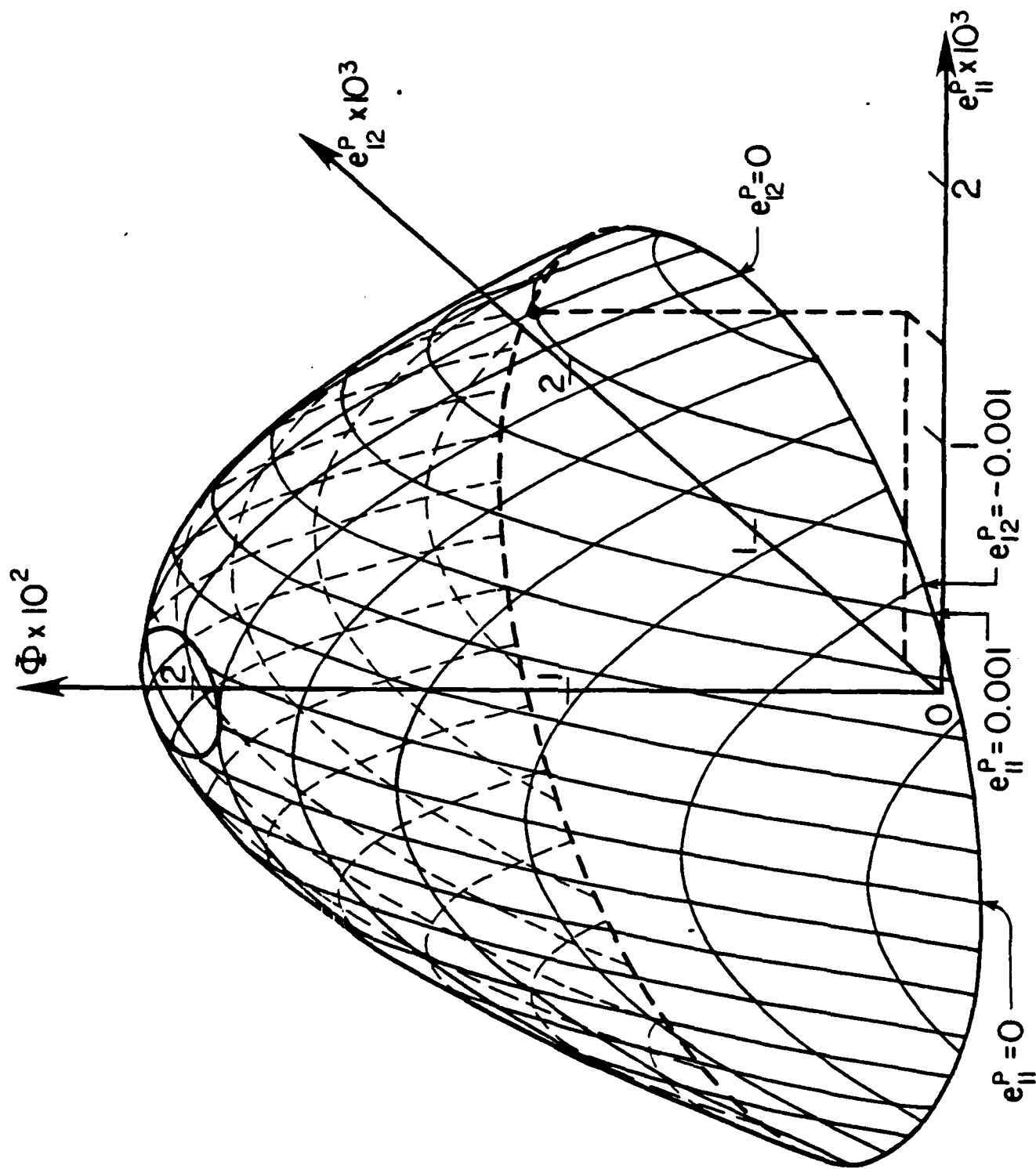


Fig. 4

END

FILMED

1-86

DTIC